Multimode Dielectric Resonator for Accurate Determination of Frequency and Temperature Dependence of Complex Permittivity in Small, High-Permittivity Cylinders

Nikki Tagdulang, Patrick Krkotić, *Member, IEEE*, Albert Diez-Comas, *Graduate Student Member, IEEE*, Montse Pont, and Juan Manuel O'Callaghan, *Senior Member, IEEE*

***Abstract*— We present a technique to measure permittivity and loss tangent in high-permittivity cylinders. This method utilizes a resonator to conduct concurrent measurements at the three lowest quasi-TE_{01p} modes across various temperatures, combined with an algorithm to fit the loss tangent dependence on frequency and temperature. Our technique serves as a preliminary step to characterize dielectrics used in Hakki–Coleman resonators for surface resistance measurements. Consequently, parameters for dielectric characterization—such as sample size and modes used—are determined by the requirements of subsequent surface resistance measurements, rather than optimizing the determination of the material's intrinsic dielectric properties. Despite this focus, our measurements on rutile align well with existing literature. We conducted measurements on three rutile samples from the same production batch, covering a frequency range from 6.0 to 9.4 GHz, with uncertainties of less than 0.7% for permittivity and 13% for loss tangent. These measurements revealed sample-to-sample differences that cannot be attributed to measurement uncertainty alone. Our findings suggest that the previous approach of using multiple rutile crystals with varying sizes to assess the frequency dependence of dielectric loss may lead to significant uncertainty in predicting loss tangents due to variations in sample properties. We describe the possible extension of this technique to characterize other dielectrics beyond rutile, including commercial dielectrics, across frequency and temperature. We also discuss its potential widespread application in the use of Hakki–Coleman resonators for quality control of materials used in particle accelerators, such as the future circular collider hadron-hadron (FCC-h).**

Received 14 June 2024; revised 16 September 2024; accepted 24 September 2024. Date of publication 3 January 2025; date of current version 8 January 2025. This work was supported by CERN under Grant FCC-GOV-CC-0210 (KE4945/ATS) and Grant FCC-GOV-CC-0209 (KE4946/ATS). The work of Nikki Tagdulang was supported for the Ph.D. Scholarship under Grant MSCA-COFUND-2016-754397. The Associate Editor coordinating the review process was Dr. Yuan Gao. *(Corresponding author: Juan Manuel O'Callaghan.)*

Nikki Tagdulang is with ALBA Synchrotron Light Source, 08290 Barcelona, Spain, and also with the CommSensLab, Department of Signal Theory and Communications, Universitat Politècnica de Catalunya (UPC), 08034 Barcelona, Spain (e-mail: nikki.tagdulang@upc.edu).

Patrick Krkotić is with the Technology Department, CERN, 1211 Geneva, Switzerland (e-mail: patrickkrkotic@outlook.de).

Albert Diez-Comas is with UN Lab, Department of Electrical and Computer Engineering, Northeastern University, Boston, MA 02115 USA (e-mail: diezcomas.a@northeastern.edu).

Montse Pont is with ALBA Synchrotron Light Source, 08290 Barcelona, Spain (e-mail: pont@cells.es).

Juan Manuel O'Callaghan is with CommSensLab, Department of Signal Theory and Communications, Universitat Politècnica de Catalunya (UPC), 08034 Barcelona, Spain (e-mail: joan.ocallaghan@upc.edu).

Digital Object Identifier 10.1109/TIM.2024.3522383

***Index Terms*— Dielectric resonator, loss tangent, dielectric loss, permittivity rutile, titanium dioxide.**

I. Introduction

HAKKI–COLEMAN resonators are test devices used for measuring surface impedance, particularly in superconductors [1], [2]. These resonators employ a dielectric cylinder to isolate electromagnetic fields from the cavity walls, ensuring that losses primarily stem from the samples under examination. The dielectric material must exhibit moderate-to-high permittivity and low dielectric loss to achieve this goal. Typically, sapphire is the preferred material due to its very low loss tangent. However, when constraints related to size or low-frequency measurements arise, alternative dielectrics with higher permittivities, such as rutile (TiO_2), become necessary. Although rutile offers a very high permittivity, its dielectric loss is significantly higher than that of sapphire, necessitating experimental characterization to obtain accurate surface impedance measurements [3].

The significance of Hakki–Coleman resonators using high-permittivity dielectrics has increased due to the potential use of high-temperature superconductor coated conductors (HTS-CC) in future particle colliders [4], [5] such as the future circular collider hadron-hadron (FCC-hh) [6] and the Chinese Super Proton–Proton Collider (SPPC) [7]. HTS-CCs, fabricated on narrow tapes, could be extensively utilized in these colliders if their surface resistance proves to be significantly lower than that of copper at the relevant particle bunch spectra (from dc to 2 GHz). Testing surface resistance at these frequencies on small samples necessitates the use of high-permittivity dielectrics with low dielectric loss. Moreover, the requirement for low surface resistance must be met in the presence of strong dc magnetic fields (up to 16 T in the FCC-hh), which demands cryogenic surface resistance measurements in magnets with limited bore sizes. This further emphasizes the need for compact test assemblies and high-permittivity dielectrics.

This study aims to characterize the permittivity and loss tangent of rutile crystals across a range of frequencies and temperatures pertinent to the aforementioned applications. This capability is often lacking among crystal vendors. This dielectric characterization is a crucial preliminary step to

surface resistance measurements, requiring the same crystals to be used in both processes with modes having similar electromagnetic field distributions (TE modes). This approach stands in contrast to previous studies focused on intrinsic dielectric properties, where experimental conditions—such as sample dimensions, mode selection, and control over sample composition and crystallographic orientation—were tailored to optimize the experimental determination of dielectric properties.

Despite the distinct objectives, our techniques and results can be compared to previous measurements on the same dielectric material. Our method circumvents the need for multiple rutile specimens, as used in some earlier studies, thereby reducing potential experimental uncertainty due to sample-to-sample variations.

The dielectric characterization method presented in this study also holds potential applications in the telecom industry. Dielectric cylinders used in this industry are manufactured by sintering various ceramic powders to achieve high permittivity with temperature stability. As with our work, these cylinders are not designed to characterize material properties, yet quality control could benefit from the theories and procedures detailed in this article.

This article is organized as follows. Section II describes the materials and methods used to determine permittivity and loss tangent from the measurement of resonance frequency and quality factor in our set of cavity resonators. Section III details the theoretical background to derive loss tangent from quality factor measurements, to perform a least-squares fit of loss tangent versus frequency and temperature, and to quantify uncertainties both in the experimental measurement and in the least-squares fit. Section IV describes the results obtained on a set of rutile crystals from a single manufacturing batch. Section V we confirm the advantages of our technique over other ones and confirm its validity by comparing our results to those obtained by other methods and those predicted theoretically. Additionally, we have included two appendices: one detailing the calculation of uncertainties, and another demonstrating that the devices shown in Section II and the theory described in Section III can be applied to characterize commercial dielectrics across different temperatures and frequencies.

II. Material and Methods

A. Dielectric Resonators and Measurement Setup

Our measurement technique uses two different dielectric resonator configurations having a common external cylindrical copper cavity (see Fig. 1). Combined measurements of resonance frequency and quality factor on both cavities are used to determine the permittivity and loss tangent of the dielectric under test (DUT)—rutile in our case. Fig. 1(a) shows the parts of the resonator shown in Fig. 1(b), corresponding to a multimode configuration containing the DUT, while Fig. 1(c) shows a single-mode configuration used to characterize the losses of the copper cavity. To aid in the precise centering of the sapphire supports, the cavity bottom incorporates a shallow circular recess (not shown in the figure) with a diameter of 4 mm and a depth of less than 0.1 mm, aligned with the cavity axis. This recess is visible through the sapphire,

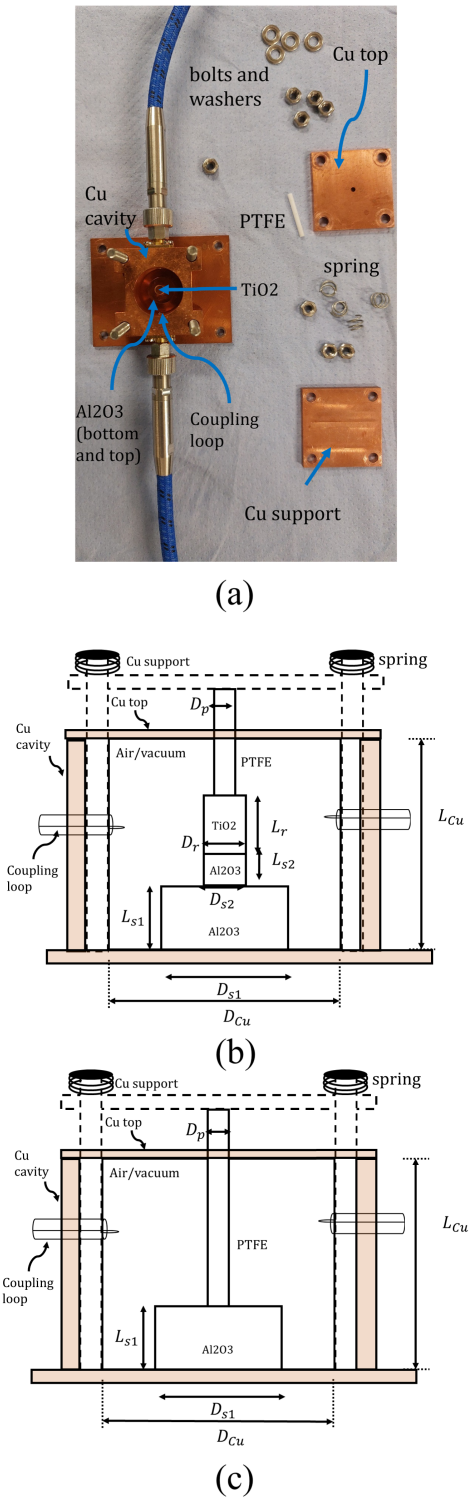

Fig. 1. Schematics of the shielded copper cavity, with the two configurations used in this work. (a) Parts of the resonator showing the dielectrics mounted inside the copper cavity. (b) Multimode quasi-TE_{01p} arrangement to asses dielectric properties of rutile. (c) Single-mode configuration to measure parasitic metal losses. The dimensions shown in the figure are the cavity diameter $D_{\mathrm{Cu}} = 19.94$ mm and length $L_{\mathrm{Cu}} = 22.10$ mm, larger sapphire (Al_2O_3) diameter $D_{S1} = 12.00$ mm and length $L_{S1} = 6.02$ mm, smaller sapphire diameter $D_{S2} = 4.04$ mm and length $L_{S2} = 3.10$ mm, and PTFE diameter of $D_p = 2.1$ mm. The diameters D_r and lengths L_r of the rutile under test (DUT) are given in Table I.

serving as a guide for manual centering. These resonators are mounted on the cold head of a Janis cryostat cooled with a Gifford-McMahon closed-cycle refrigerator for low-temperature measurements. The measurement set-up is shown in Fig. 2. An Agilent TwisTorr 74 FS turbomolecular pump with a Scroll IDP15 primary pump and a Leybold Thermovac TTR 911 N vacuum gauge are used to evacuate the cryostat and monitor the pressure. A Lakeshore 321 temperature controller is connected to a DT-470 silicon diode temperature sensor and heater in the cold head. A thermocouple, connected to a second channel of the Lakeshore 335 temperature controller, is attached at the top of the cavity to monitor thermal gradients. Differences in readings between this thermocouple and the sensor in the cold head are kept below 0.8 K. To ensure consistency in our temperature settings, we performed three cycles of cavity assembly, cooldown, and resonance frequency measurements at various temperature setpoints. The relative differences observed across these cycles were within the limits of our resonance frequency uncertainty.

Semi-rigid cables terminated with 3.5 mm connectors are used between the cryostat feedthroughs and the dielectric resonator. Flexible test cables terminated with 3.5 mm connectors are also used to connect the cryostat feedthroughs and the Rohde & Schwarz ZNA26 vector network analyzer that measures the S-parameters. A full two-port calibration using Rohde & Schwarz ZN-Z53 Calibration kit is performed at the end of the semi-flexible cables. The effect of the semirigid cables inside the cryostat is taken into account in a post-processing algorithm (ARPE, see [8]). A computer with Python-based software is used to automatically control the temperature and acquire S-parameter data. The software ensures the S-parameters are centered about the resonance frequency of the quasi-TE_{01p} modes with 401 points per sweep. The frequency span is set close to ten times the 3 dB bandwidth (see details in [8]). To ensure temperature-stable measurements, the frequency and unloaded quality factor are continuously monitored as the dielectric resonator is cooled down and stabilized to a minimum temperature of 30 K. Complete stabilization is confirmed when successive measurements of the resonance frequency and quality factor show no time-dependent trend at this temperature. Once stabilized, the S-parameters are acquired at 1 K intervals with a temperature ramp of 0.5 K/min, allowing for 1-min stabilization at each temperature set point.

The cavity in Fig. 1(b), is based on previous designs [9], [10], adapted for measurements of small high-permittivity dielectric cylinders. A set of external springs applies pressure on a PTFE rod that holds the rutile DUT on top of a pair of sapphire crystals. The cavity is fed with adjustable coupling loops to couple with the three lowest quasi-TE_{01p} modes, which we will refer to as TE_{011}, TE_{012}, and TE_{013}. This design minimizes uncertainty in loss tangent determination by maximizing the contribution of the DUT loss to the overall cavity loss while providing mechanical stability and good thermal contact between the DUT and the external copper cavity. Quantitative details on the contribution of DUT loss on the overall cavity loss are given in Section III-A.

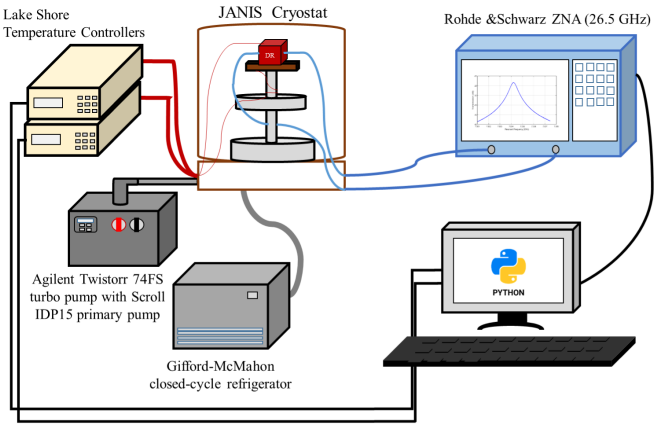

Fig. 2. Measurement setup.

The DUT permittivity is determined by matching the resonance frequency obtained from electromagnetic simulations with that obtained in the measurements. Accurate DUT dimensions have to be entered in the simulations since these—besides permittivity—greatly affect the resulting resonance frequency.

The loss tangent of the DUT is determined from the quality factors of both cavities following a procedure described in Section III-A that takes into account the dimensions of both configurations and the size and permittivity of all dielectrics in them.

B. Determination of Unloaded Quality Factor and Resonance Frequency

Experimental determination of the unloaded quality factor (Q_0) and resonance frequency (f_0) is needed to calculate the DUT's loss tangent and permittivity. These parameters can be readily determined in a weakly coupled resonator exhibiting a Lorentzian transmission response [11] but, as in other cavity-based dielectric characterization methods [10], [12], the transmission responses of the modes used might have asymmetries, as shown in Fig. 3.

To determine the characteristic resonator parameters and overcome possible asymmetries, we use ARPE [8], an open-source, web-executable code that fits the frequency response of the cavity's complex transmission and reflection coefficients and extracts the resonator parameters, including Q_0 and f_0. The algorithm in ARPE can compensate for the parasitic cross-coupling between the cavity's input and output ports (usually causing asymmetries) and the effect of the input and output loading on the resonator quality factor. The algorithm also includes an adaptive outlier removal routine capable of rejecting measurement points that do not conform to the expected resonator response due to defects in the measurement setup. ARPE's combination of least-squares fitting for the frequency response and adaptive outlier removal has proven highly effective in mitigating the minor effects of compressor vibrations on the resonators' frequency response. Due to the shorter vibration period compared to the frequency sweep duration, small ripples may occasionally appear in the

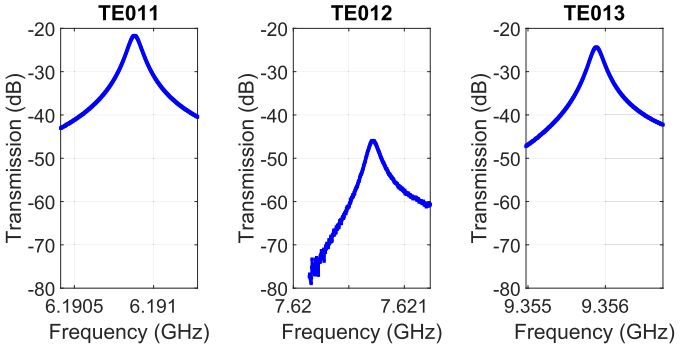

Fig. 3. Transmission frequency response for the three quasi-TE_{01p}-modes with a frequency span of ten times the half-power bandwidth at 95 K.

S-parameter response. In addition, small clusters of measurement points sometimes deviate from the overall measurement trend. Despite these infrequent perturbations, ARPE consistently extracts the resonance frequency and quality factor.

ARPE's ability to accurately extract resonator parameters across a range of coupling levels (as shown in Fig. 3) allows for concurrent multimode measurements without the need to adjust the coupling for each mode. This eliminates the requirement for a coupling adjustment mechanism within the cryogenic system.

In addition, ARPE is optimized for handling large datasets, such as those needed to analyze the data presented in the figure. Our data acquisition software generates three S-parameter files (.s2p), each containing 401 frequency points, at each temperature setpoint. These files can be simultaneously uploaded to the ARPE platform, which outputs .CSV files with coupling factors, quality factors, and resonance frequencies—streamlining experimental data processing.

The uncertainties associated with data fitting using ARPE are generally small compared to other sources of experimental uncertainty. When the cavity remains undisturbed, ARPE typically yields uncertainties in Q_0 at fractions of a percent and uncertainties in f_0 at approximately one-tenth of the half-power bandwidth [8].

III. Theory

A. Loss Tangent Determination

The dielectric loss tangent of the crystals for each mode in the multimode cavity [see Fig. 1(b)] is computed from the measured unloaded quality factor Q_0, the dielectric filling factor p_r [10], and the parasitic quality factor Q_p from the losses not due to the DUT

$$\tan\delta_r = \frac{1}{p_r}\left(\frac{1}{Q_0} - \frac{1}{Q_p}\right). \tag{1}$$

We evaluate the dielectric filling factor p_r with a 3-D electromagnetic simulation performed with CST's Microwave Studio Eigenmode Solver [13], which uses a finite element method to solve for the field solutions of the set-up in Fig. 1(a). This software can post-process the field distribution to determine the unloaded quality factor Q_0. In the simulation, we assume that all materials are lossless except for the DUT. In these conditions $1/Q_p = 0$ in (1) and one can obtain p_r by relating $\tan\delta_{r,\mathrm{CST}}$—an arbitrary (but plausible) user-defined value of loss tangent entered as a simulation parameter in CST—, with the Q_0 resulting from the simulation. The subscripts CST used henceforth will denote similar user-defined simulation parameters entered in CST.

Parasitic losses are produced in the copper cavity, PTFE rod, and sapphire supports. Accordingly, the reciprocal of Q_p in (1) can be split into three terms

$$\frac{1}{Q_p} = p_p \tan\delta_p + p_s \tan\delta_s + \frac{R_{s,\mathrm{Cu}}}{G_{s,\mathrm{Cu}}} \tag{2}$$

where $p_p \tan\delta_p$ and $p_s \tan\delta_s$ quantify the contribution of the PTFE rod and sapphire crystals to the overall Q_0 through their filling factors (p_p and p_s respectively) and loss tangents ($\tan\delta_p$ and $\tan\delta_s$), while $R_{s,\mathrm{Cu}}/G_{s,\mathrm{Cu}}$ is the copper contribution, which depends on its surface resistance ($R_{s,\mathrm{Cu}}$) and the cavity's surface geometrical factor $G_{s,\mathrm{Cu}}$. Evaluation of p_p and p_s is done following the same procedure as that used for p_r. A very similar approach is used for the geometrical factor $G_{s,\mathrm{Cu}}$, which is determined by performing simulations considering only losses in the metal wall and calculating $G_{s,\mathrm{Cu}}$ as $G_{s,\mathrm{Cu}} = R_{s,\mathrm{CST}} Q_0$, where $R_{s,\mathrm{CST}}$ is entered as a simulation parameter and Q_0 is determined by post-processing the field distribution obtained by CST.

An accurate evaluation of parasitic loss requires an independent measurement of the surface resistance of the copper walls [14]. This is accomplished by measuring the quality factor of the cavity depicted in Fig. 1(c). As the primary loss in this cavity is attributed to its copper walls and all other sources of loss are negligible, we can consider the reciprocal of the quality factor to be proportional to the surface resistance. As in (2), this proportionality can be characterized with a geometric factor whose value can be determined through CST simulations.

The frequency used to measure the surface resistance with the single-mode cavity in Fig. 1(c) is 9.7 GHz and differs from the frequencies of the TE_{01p} modes used in the multimode cavity shown in Fig. 1(b) (spanning from 6.0 to 9.4 GHz). Consequently, to calculate the parasitic loss in (2), the value of $R_{s,\mathrm{Cu}}$ needs to be adjusted to the proper mode frequency by considering its frequency dependence. For high-purity copper, this adjustment may involve accounting for the anomalous skin effect within specific temperature ranges [15], [16]. Otherwise, a square root frequency dependence can be assumed.

It is obvious from (1) to (2) that minimizing parasitic losses will make the reciprocal of Q_p in (1) small compared to that of Q_0 and this will minimize the contribution of parasitic loss to the uncertainty in $\tan\delta_r$. The extent to which DUT losses are dominant can be quantitatively assessed by the DUT power fraction (PF) [17], which is the ratio of the DUT losses to the overall resonator losses

$$\mathrm{PF} = \frac{p_r \tan\delta_r}{1/Q_0}. \tag{3}$$

PFs have been estimated for all sources of loss in the cavity. Fig. 4 shows the various PFs for the three modes considered as a function of the expected loss tangent. The validity of the cavity design is based on the dominance of the DUT PF, which ensures a good measurement uncertainty for all three modes,

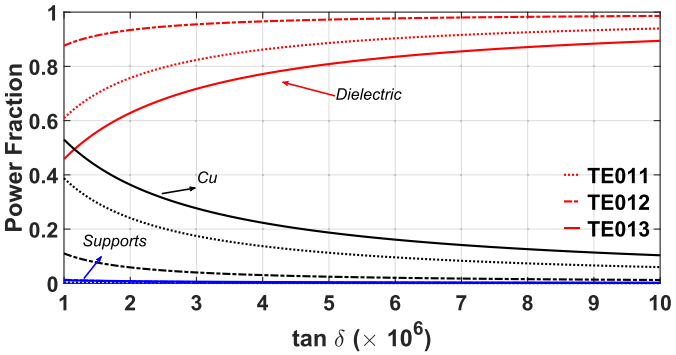

Fig. 4. PF of the different sources of loss: DUT (red), Cu cavity (black), and supports (blue), for each quasi-TE_{01p}-mode at 50 K.

although the TE_{012} mode is the one having the highest DUT PF. As will be discussed in Section III-C, the other modes are needed for a proper frequency dependence fit despite their worse DUT PFs and the impact of a mode-dependent uncertainty is minimized by properly weighting the measured data in the least-squares fitting procedure. The contributions of the sapphire and PTFE components are included in the PF labeled as "supports" in Fig. 4. To estimate these contributions, we adopted very conservative assumptions. For single-crystal sapphire, we used data from the worst-performing sample in [18] and extrapolated its performance to our resonator's frequencies, assuming the loss tangent varies with the square of the frequency [18]. For PTFE, measurements of the dielectric loss tangent at 19 GHz in [19] reported values below 10^{-5} at temperatures under 100 K. To maintain conservatism, we assumed a PTFE loss tangent an order of magnitude higher in all modes. Despite this overestimation for both PTFE and sapphire, the small filling factor and the intrinsically low loss of these materials make their contribution negligible compared to other sources of loss, even at temperatures up to 100 K. As a result, PTFE and sapphire losses were excluded from both the sensitivity analysis and the calculation of the overall loss tangent.

B. Uncertainty Analysis

The square of the uncertainty in the dielectric loss tangent can be derived from (1) to (2)

$$\left(\frac{u_{\tan\delta_r}}{\tan\delta_r}\right)^2 = \left(\frac{u_{p_r}}{p_r}\right)^2 + \frac{1}{(p_r\tan\delta_r)^2}\frac{1}{Q_0^2}\left(\frac{u_{Q_0}}{Q_0}\right)^2 + \frac{1}{(p_r\tan\delta_r)^2}\left(\frac{R_{s,\mathrm{Cu}}}{G_{s,\mathrm{Cu}}}\right)^2\left[\left(\frac{u_{G_{s,\mathrm{Cu}}}}{G_{s,\mathrm{Cu}}}\right)^2 + \left(\frac{u_{R_{s,\mathrm{Cu}}}}{R_{s,\mathrm{Cu}}}\right)^2\right] \quad (4)$$

where u_x denotes the uncertainty in parameter x. Note that, as discussed above, we have omitted the contributions of the sapphire and PTFE pieces.

Determining the uncertainty in permittivity is more complex. The permittivity of the DUT is determined by comparing the measured resonance frequency of each mode to the frequency obtained through electromagnetic simulations. The simulations take into account the dimensions of the multimode cavity and the dimensions and permittivities of all dielectric materials present inside it. As a result, the final determination of the DUT permittivity relies on the implicit functional dependence established through these simulations on all the parameters defining the multimode cavity [10]

$$\epsilon_r = F(f_0, D_r, L_r, D_{s1}, L_{s1}, D_{s2}, L_{s2} \; D_p, L_p, D_{\mathrm{Cu}}, L_{\mathrm{Cu}}, \epsilon_s, \epsilon_p) \quad (5)$$

where f_0 stands for the resonance frequency, D and L stand for the diameter and axial length of the various objects in the cavity: DUT (D_r and L_r), Cu cavity (D_{Cu} and L_{Cu}), bottom sapphire support (D_{s1}, L_{s1}), top sapphire support (D_{s2}, L_{s2}), PTFE rod (D_p, L_p), ϵ_s is the sapphire relative permittivity, and ϵ_p is the PTFE relative permittivity. The square of the uncertainty in DUT permittivity can be written as

$$\begin{aligned}\left(\frac{u_{\epsilon_r}}{\epsilon_r}\right)^2 &= S_{Dr}^2\left(\frac{u_{D_r}}{D_r}\right)^2 + S_{Lr}^2\left(\frac{u_{L_r}}{L_r}\right)^2 \\ &+ S_{Ds1}^2\left(\frac{u_{D_{s1}}}{D_{s1}}\right)^2 + S_{Ls1}^2\left(\frac{u_{L_{s1}}}{L_{s1}}\right)^2 \\ &+ S_{Ds2}^2\left(\frac{u_{D_{s2}}}{D_{s2}}\right)^2 + S_{Ls2}^2\left(\frac{u_{L_{s2}}}{L_{s2}}\right)^2 \\ &+ S_{D\mathrm{Cu}}^2\left(\frac{u_{D_{\mathrm{Cu}}}}{D_{\mathrm{Cu}}}\right)^2 + S_{L\mathrm{Cu}}^2\left(\frac{u_{L_{\mathrm{Cu}}}}{L_{\mathrm{Cu}}}\right)^2 \\ &+ S_{\epsilon_s}^2\left(\frac{u_{\epsilon_s}}{\epsilon_s}\right)^2 + S_{\epsilon_p}^2\left(\frac{u_{\epsilon_p}}{\epsilon_p}\right)^2 \\ &+ S_{Dp}^2\left(\frac{u_{D_p}}{D_p}\right)^2 + S_{Lc}^2\left(\frac{u_{L_p}}{L_p}\right)^2 + S_f^2\left(\frac{u_{f_0}}{f_0}\right)^2 \quad (6)\end{aligned}$$

where the sensitivity coefficients [10] are defined as $S_z = (\partial\epsilon_r/\partial z)(z/\epsilon_r)$ and z denotes the subscripts in (5).

Since the DUT samples are high-permittivity dielectrics, most of the electromagnetic fields are confined within the DUT. All supports are made of low-permittivity dielectrics and are designed such that their effect on the frequencies of the TE_{01p} modes is negligible. The Cu cavity is also designed such that all of its walls are well away from the DUT. Thus, the uncertainties due to the dimensions of the Cu cavity, supports, ϵ_s, and ϵ_p are considered to be negligible. Consequently, (6) simplifies into

$$\left(\frac{u_{\epsilon_r}}{\epsilon_r}\right)^2 = S_{Dr}^2\left(\frac{u_{D_r}}{D_r}\right)^2 + S_{Lr}^2\left(\frac{u_{L_r}}{L_r}\right)^2 + S_f^2\left(\frac{u_{f_0}}{f_0}\right)^2. \quad (7)$$

The sensitivity coefficients related to dimensions (diameters and lengths) are determined numerically through two sets of simulations. In the first set, a linear relationship is established between perturbations in a specific dimension and the resulting perturbation in frequency. The second set of simulations establishes the perturbation in DUT permittivity that corresponds to the earlier frequency perturbation.

C. Loss Tangent Dependence on Temperature and Frequency

Our approach allows the concurrent measurement of three specific frequencies, corresponding to the TE_{011}, TE_{012}, and TE_{013} modes of the cavity, at every temperature setpoint for an individual dielectric sample. The resulting data are then fit to the following equation [18], [20], [21]:

$$\tan\delta = \alpha f^{\beta} T^{\gamma} \tag{8}$$

where T is the temperature and α, β, and γ are fitting parameters. Equation (8) can be transformed to a linear combination by taking the natural logarithm on both sides of the equality

$$\ln(\tan\delta) = \ln(\alpha) + \beta\ln(f) + \gamma\ln(T) \tag{9}$$

from which we can build a matrix equation $Ax = b$ of the form

$$\begin{pmatrix} 1 & \ln(f_1) & \ln(T_1) \\ 1 & \ln(f_2) & \ln(T_2) \\ 1 & \cdot & \cdot \\ 1 & \cdot & \cdot \\ 1 & \ln(f_n) & \ln(T_n) \end{pmatrix} \begin{pmatrix} \ln(\alpha) \\ \beta \\ \gamma \end{pmatrix} = \begin{pmatrix} \ln(\tan\delta_1) \\ \ln(\tan\delta_2) \\ \cdot \\ \cdot \\ \ln(\tan\delta_n) \end{pmatrix} \tag{10}$$

where the subscripts $i = 1, \ldots, n$ refer to all temperature and frequency pairs used in the measurement. Loss tangent uncertainty is the main contribution to the fitting error between the left and right-hand side of (10). The resulting uncertainties in α, β, and γ can be found using error propagation techniques in matrix computations [22]. To apply these techniques, we consider the effect of relative perturbations ζ_i in the values of $\tan\delta_i$ in (10). Since $\ln(1+\zeta_i) \approx \zeta_i$ for $\zeta_i \ll 1$ these perturbations will generate an additional column vector in the right-hand side of (10) which will, in turn, cause perturbations in the fitting parameters α, β, and γ. The best estimate for these parameters is obtained when the equations in (10) are normalized to the measurement uncertainty. Accordingly, a weighting matrix W_0 is applied to (10) to transform it from $Ax = b$ to $W_0Ax \approx W_0b$ with $W_{0ii} = 1/\zeta_i$ and $W_{0ij} = 0$ for $i \neq j$. In these conditions, the least squares fit solution is given by

$$x = (A^T W_0^2 A)^{-1} A^T W_0 b \tag{11}$$

and the uncertainties in the fitting parameters α, β, and γ can be found from the diagonal terms of the covariance matrix

$$G_{xx} = (A^T W_0^2 A)^{-1} \tag{12}$$

where the normalization coefficients are $\zeta_i = u_{\tan\delta_i}/\tan\delta_i$ calculated from (4) at each frequency and temperature pair.

IV. Results and Discussion

A set of three c-oriented rutile single crystals belonging to the same batch provided by Alineason Materials Technology GmbH [23] was studied. The purity of the crystals is above 99.98%. The dimensions of the crystals are given in Table I. The axis of the crystal cylinder is aligned with the axis of the cavity and perpendicular to the electric field; thus, the perpendicular components of the loss tangent and permittivity are measured.

TABLE I
Rutile Dimensions for Each Crystal at Room Temperature

Parameters	rutile A	rutile B	rutile C
D_r (mm)	4.04 (1)	4.08 (1)	4.04 (1)
L_r (mm)	5.55 (1)	5.55 (1)	5.55 (1)

A. Permittivity

As mentioned in Section III-B, the sensitivity coefficients in (7) are calculated through two sets of electromagnetic simulations relating changes in the resonance frequency produced by perturbations in the parameters in (5). To validate this approach, a verification process was undertaken to examine the conditions under which the resonance frequency obtained through these electromagnetic simulations could be properly used in this assessment.

For the verification, a Hakki–Coleman resonator with a dielectric having the following specific dimensions was used: diameter of 4.08 mm, length of 5.55 mm, and a relative permittivity of 110 (published ϵ_r data at 35 K [9]). This resonator also holds TE_{011}, TE_{012}, and TE_{013} modes with resonance frequencies ranging from 6.5 to 10.4 GHz. These frequencies can be determined by solving a transcendental equation [24], which can be subsequently compared to those resulting from an electromagnetic simulation.

The verification was done on the three modes. Absolute relative differences between the frequencies derived from the transcendental equation and those obtained from the simulation were below $4 \cdot 10^{-5}$ for the three modes when the simulations were performed with at least 100 000 mesh cells. In the simulations of the resonator in Fig. 1, we have used about 200 000 mesh cells, equivalent to a minimum edge length of 0.02 mm, to be well below these differences. The simulations above have been performed using eigenmode simulations with perfect conducting walls (PEC) in CST. We have verified that the differences in resonance frequency are negligible when PEC walls are substituted by lossy copper walls, when coupling loops are included in the simulation, and when the CST simulation method is changed from eigenmode to frequency domain. In addition, we assessed $u_{f_0}/f_0 \approx 6 \cdot 10^{-4}$ by assembling and disassembling the cavity ten times, measuring its resonance frequency at room temperature after each assembly and taking the ratio between the resulting standard deviation and average. We also confirmed this result at low temperatures by performing three assembly-measurement-disassembly sequences.

In conclusion, the term u_{f_0}/f_0 in (7) is dominated by the uncertainties related to the assembly and disassembly of the cavity and not by those due to the simulation. This applies both to the comparison with the Hakki–Coleman resonator and also to the various CST simulation options.

All sensitivity coefficients in (7) were calculated through electromagnetic simulations between 30 and 110 K which corresponds to the temperature range of interest in this study. Table II lists the magnitude of the sensitivity coefficients at 30 and 110 K. We found that $|S_f|$ is close to 2 [12], proving the approximate proportionality of resonance frequency with $1/\sqrt{\epsilon_r}$ for high permittivity dielectrics.

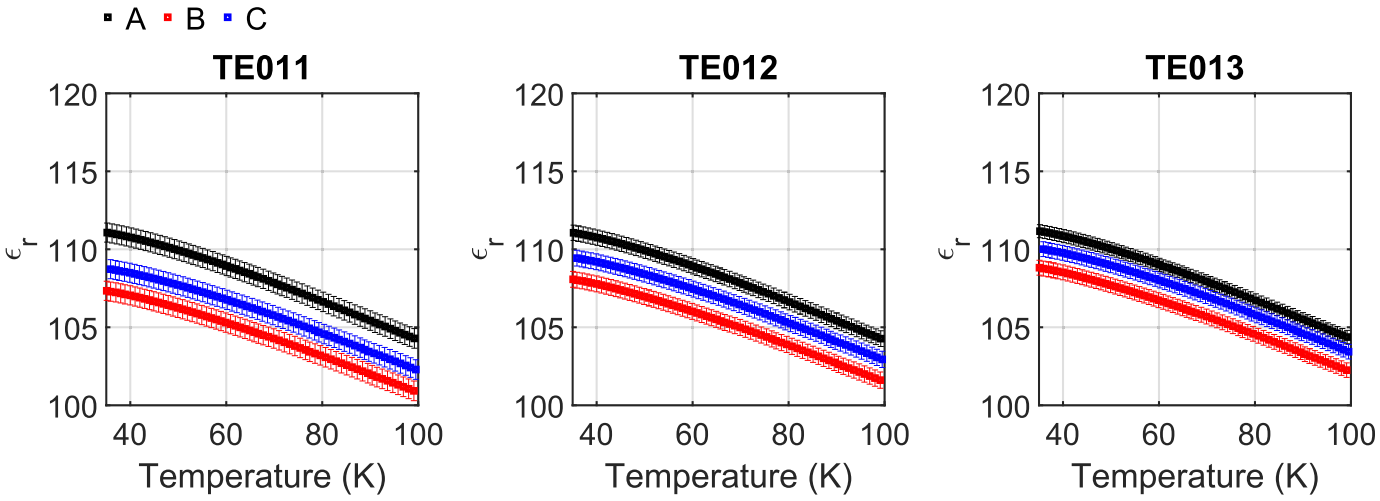

Fig. 5. Relative permittivity in all crystals versus temperature for TE_{011}, TE_{012}, and TE_{013} modes.

TABLE II
SENSITIVITY COEFFICIENTS AT 30 AND 110 K (INSIDE PARENTHESES) FOR EACH MEASURED MODE

Parameters	$\lvert S_D \rvert$	$\lvert S_L \rvert$	$\lvert S_f \rvert$
TE_{011}	1.733 (1.939)	0.246 (0.275)	2.009 (2.252)
TE_{012}	1.328 (1.485)	0.642 (0.717)	1.993 (2.235)
TE_{013}	1.055 (1.093)	0.988 (1.017)	2.090 (2.335)

The resonance frequency is also influenced by the thermal expansion of the cavity components (mainly by the DUT crystal). In our simulations, relative permittivity was determined using the dimension of each crystal at room temperature. Thus, the terms u_{D_r} and u_{L_r} are attributed to the uncertainty in dimensions measured at room temperature ($u_{D_r,\mathrm{RT}}$ and $u_{L_r,\mathrm{RT}}$) combined with the uncertainty due to changes in temperature ($u_{D_r,\mathrm{LT}}$ and $u_{L_r,\mathrm{LT}}$).

To assess the contribution from $u_{D_r,\mathrm{RT}}$ and $u_{L_r,\mathrm{RT}}$, we used the specifications of the micrometer combined with random uncertainty from the operator and reproducibility at room temperature measurements; $u_{D_r,\mathrm{RT}} = 0.01$ mm and $u_{L_r,\mathrm{RT}} = 0.01$ mm. Table I presents the dimensions of each crystal at room temperature.

To assess the uncertainty from $u_{D_r,\mathrm{LT}}$ and $u_{L_r,\mathrm{LT}}$, we use the published values of thermal expansion at 100 K [25] and 4 K [26] both defined with respect to room temperature. The thermal expansion of rutile has a weak temperature dependence between these two temperatures and we take the most unfavorable value to make a conservative uncertainty estimate for both $D_{r,\mathrm{LT}}$ and $L_{r,\mathrm{LT}}$ which are $u_{D_r,\mathrm{LT}}/D_{r,\mathrm{LT}} \approx u_{L_r,\mathrm{LT}}/L_{r,\mathrm{LT}} \approx 0.2\%$. With this, the total relative uncertainties in rutile dimensions are $u_{D_r}/D_r = 0.4$ % and $u_{L_r}/L_r = 0.3\%$, comprising 95% of the uncertainty in ϵ_r. As a result, the relative uncertainty in ϵ_r is nearly temperature-independent and below 0.7%, in all crystals. This uncertainty is comparable with that of similar techniques intended for larger crystals compared to our specimens [10], [12] and is an order of magnitude lower than that in [27].

Fig. 5 shows the relative permittivity (perpendicular to the crystal cylinder) as a function of temperature for all three modes in the three rutile crystals. These findings closely resemble the results reported in other works [9], [20], [28]. Furthermore, we compared these results with Hakki–Coleman DR measurements in [29] using TE_{011} mode and also found close agreement.

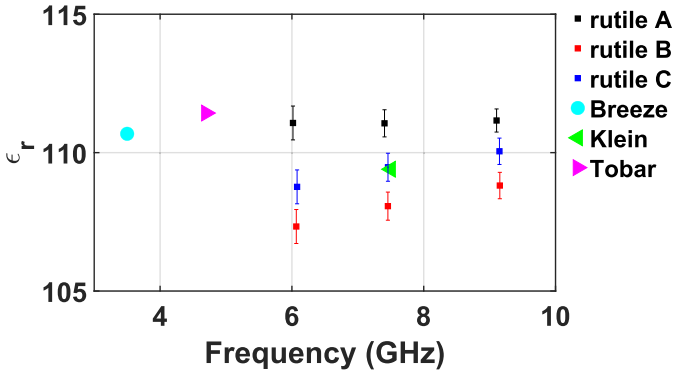

Fig. 6. Relative permittivity at 35.2 K for each crystal compared to other results in [9], [20], and [28]. Results by Sabsky and Gerritsen [30] ($\epsilon_r = 128.5$ at X-band) are not plotted because they do not quote a specific frequency.

Fig. 6 shows that ϵ_r at any given frequency is different for each crystal with the largest variation found at the lowest frequency measured. At 6 GHz, the difference between samples A and B is about 3.7 units, a factor ≈ 6 higher than the uncertainty of both samples. This implies that this technique can detect small changes in ϵ_r.

Fig. 6 also compares our results with those of other publications at 35.2 K.

B. Loss Tangent

We use (4) to evaluate the uncertainty of the loss tangent for each mode. The resonator parameters p and G_s were calculated using CST. The uncertainty of these parameters is influenced by the uncertainty in dimensions and electromagnetic simulations.

For the assessment of u_p and u_{Gs}, we employ a Hakki–Coleman resonator, in a similar fashion to what was done in Section IV-A. After analytically calculating p and

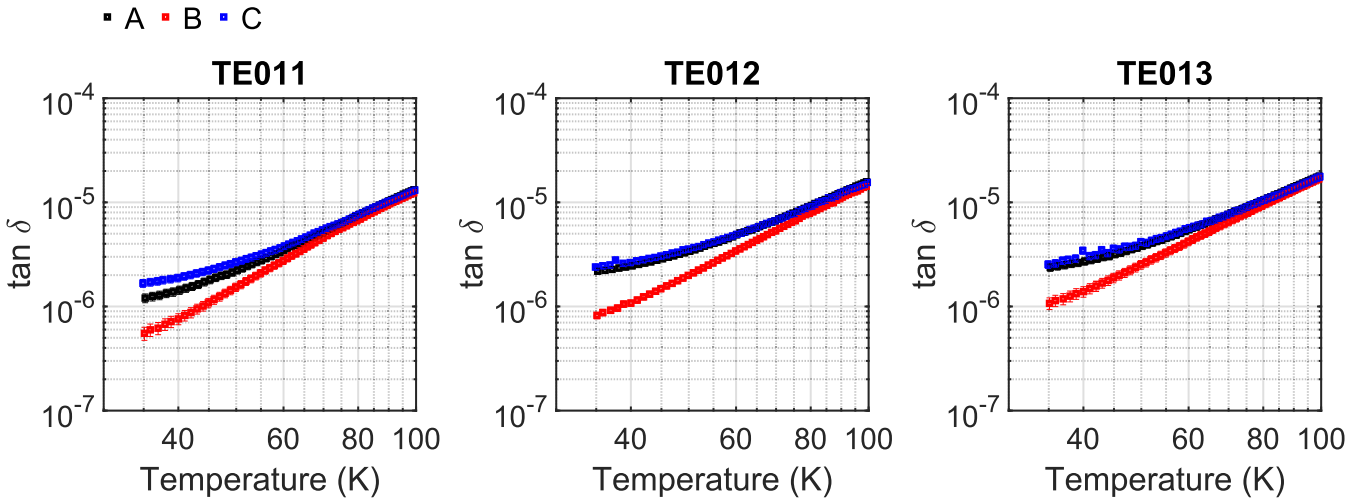

Fig. 7. Loss tangents for crystals A–C for modes TE_{011} (6.02–6.21 GHz), TE_{012} (7.41–7.65 GHz), and TE_{013} (9.11–9.38 GHz).

G_s, the results were compared to those from electromagnetic simulations conducted under the same conditions. Through this process, we found that the relative differences obtained between analytical and numerical solutions are about 2% if numerical simulations are performed using at least 100 000 mesh cells, and therefore, the contribution of numerical simulations to u_p/p and u_{G_s}/G_s is, at most, 2%.

Further, we evaluated the uncertainty of these parameters due to the uncertainty in dimensions. We found that this uncertainty is negligible on u_p/p in all modes and on u_{G_s}/G_s for TE_{011} and TE_{012}. Whereas, we calculated the upper bound of the total uncertainty of u_{G_s}/G_s (including dimensional and numerical uncertainty) to be ≈4% for TE_{013}.

The uncertainty of the quality factor (u_{Q_0}) is determined by repetitively assembling and disassembling the cavity shown in Fig. 1(a) as done with the resonance frequency. After 10 repetitions at room temperature, the resulting u_{Q_0}/Q_0 value is approximately 6%. This was confirmed at low temperatures through three repeated measurements.

To determine the relative uncertainty in surface resistance ($u_{R_s,\mathrm{Cu}}/R_{s,\mathrm{Cu}}$), we equate it to the relative uncertainty in the quality factor observed in the cavity depicted in Fig. 1(c). This equivalence is based on the fact that surface resistance is the main contributor to loss in this particular cavity, leading to an unloaded quality factor that is directly proportional to the reciprocal of the surface resistance. We obtain $u_{R_s,\mathrm{Cu}}/R_{s,\mathrm{Cu}} = 6\%$ using the same evaluation method as that used for the multimode cavity shown in Fig. 1(b). Additionally, we confirmed the accuracy of the copper surface resistance values obtained from the resonator in Fig. 1(c) by conducting a redundant measurement. This involved testing samples from the same copper block used to fabricate the cavity in a separate Hakki–Coleman resonator at 6.5 GHz.

It follows from (4) that the uncertainty in $\tan\delta$ is higher for low-loss crystals at low temperatures. For the sample with the lowest loss (rutile B), the relative uncertainties at 35 K for TE_{011}, TE_{012}, and TE_{013} modes are 15%, 8%, and 13%, respectively. We note that although we have used a smaller rutile crystal (4 mm in diameter and 5.55 mm high) compared to that of [28] (20 mm in diameter and 10 mm high) or that of [9] (10 mm in diameter and 5 mm high) which promise more sensitive measurements, we yielded reasonable uncertainty in the dielectric loss tangent.

TABLE III
FITTING PARAMETERS AND THEIR UNCERTAINTIES (IN PARENTHESES) FOR THE LOSS TANGENT DEPENDENCE ON FREQUENCY AND TEMPERATURE BETWEEN 35 AND 100 K AND 6 TO 9.2 GHZ FOR THE THREE RUTILE CRYSTALS

TiO_2	$\ln(\alpha)$	β	γ	COD
A	-44.132 (732)	1.018 (32)	2.138 (18)	0.963
B	-45.571 (823)	0.936 (36)	2.860 (20)	0.989
C	-40.585 (750)	0.900 (33)	1.942 (18)	0.984

Fig. 7 shows the loss tangent for all modes and samples as a function of temperature. It can be observed that $\tan\delta$ in all modes and samples decreases with decreasing temperature with a reduction of the slope at lower temperatures. This is consistent with the behavior observed from measurements of rutile in [18], [20], [28], and [31]. On the other hand, we obtain higher $\tan\delta$ than that reported in [20] for the same frequency range. Figs. 8 and 9 compare the values of loss tangent of our three samples with those in the literature.

In addition, differences in $\tan\delta$ are observed among different crystals. In particular, at 35 K for the TE_{012} mode, the loss tangent of sample B differs by about $1.59 \cdot 10^{-6}$ from that of sample C. This is about 20 times the $\tan\delta$ uncertainty of sample B and 11 times that of C, which suggests that this difference cannot be attributed to measurement uncertainties.

These results indicate that even if all crystals belong to the same fabrication batch, minor individual differences in their purity and/or morphology have a significant effect on their loss tangent.

We calculated the frequency and temperature dependence of $\tan\delta$ using the weighted least square fit described in Section III-C between 35 and 100 K. Table III shows the result of the fit using (8) to (11) and the uncertainties from (12).

We assessed the goodness of our fitting model using the coefficient of determination R^2 listed in Table III, obtaining values close to 1. In addition, the uncertainty of the fitting

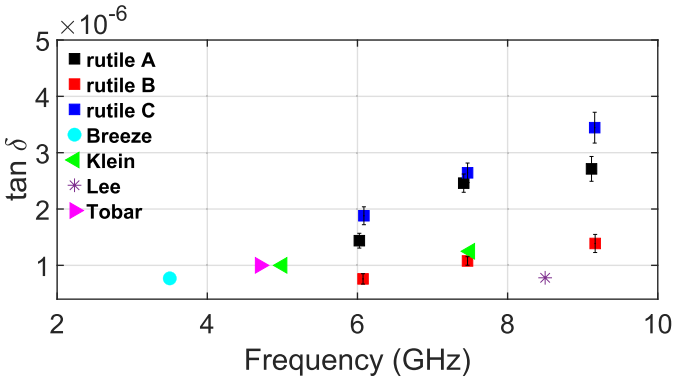

Fig. 8. Dielectric loss tangent at 40 K of samples A–C compared to previous literature [9], [20], [28], [33]. Sabisky and Gerritsen [30] (not plotted) reports $9.19{\cdot}10^{-6}$ at X-band frequencies.

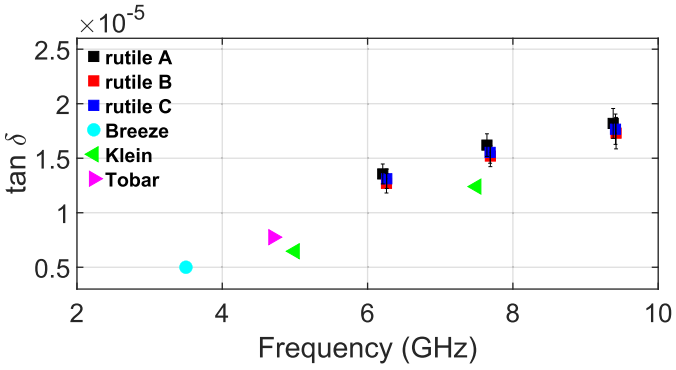

Fig. 9. Dielectric loss tangent at 100 K of samples A–C compared to previous literature [9], [20], [28]. Sabisky and Gerritsen [30] (not plotted) reports $2.40 \cdot 10^{-5}$ at X-band frequencies.

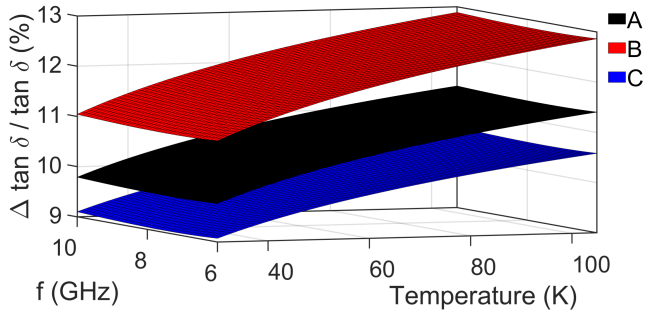

Fig. 10. $u_{\tan\delta}/\tan\delta$ versus frequency and temperature.

parameters indicated in Table III was calculated using the covariance matrix (12) whose diagonal terms are the variances of $\ln(\alpha)$, β, and γ. Using these uncertainties in (9), we can predict the uncertainty in $\tan\delta$ versus frequency and temperature. The result is shown in Fig. 10 for all crystals.

As shown in Table III, β and γ range between 0.900–1.018 and 1.942–2.860, respectively. These values do not agree with the theoretical ones for intrinsic dielectric loss of centrosymmetric crystals at low temperatures [21] ($\beta = 2$ and $\gamma = 4$), suggesting a possible dominance of extrinsic effects (such as impurities) in this behavior. To further this, we notice that the temperature dependence presents clear differences between samples, as evidenced by the large dispersion in γ values in Table III and the different slopes in the graphs in Fig. 7 below 80 K, which might also be due to defects extrinsic to the material [18]. On the other hand, the measured frequency dependence in $\tan\delta$ is quite uniform, with β ranging from 0.900 to 1.018, in accordance with the linear dependence commonly found in nonorganic ceramics at frequencies between 5 and 12 GHz [32].

Previous measurements [20] made on rutile having the same high purity at 5 and 8 GHz, and temperatures between 80 and 150 K obtained $\beta = 1.7$ and $\gamma = 2.7$. These measurements were made on two different rutile specimens using single-mode resonators to obtain data at different frequencies. The differences between the results in [20] and those in Table III may be due to differences in the samples used in the two single-mode resonators used in [20]. The temperature range chosen in [20] to fit to (8) avoids the low-temperature regime where charge carrier freeze-out occurs [31] and loss tangent becomes temperature-independent. Similar to [20], we expect the coefficients of determination in Table III to degrade if we extend the temperature range to lower values, where the loss tangent exhibits a very weak temperature dependence (particularly for samples A and C), deviating from the behavior predicted by (8).

V. Conclusion

We have developed a technique capable of accurately determining the permittivity and loss tangent in high-permittivity cylindrical dielectrics at low temperatures using three modes having frequencies between 6.0 and 9.4 GHz. The technique is not designed to obtain the intrinsic dielectric properties of the material but rather to characterize a specific dielectric cylinder that will subsequently be used in surface resistance measurements. Therefore, the conditions under which the dielectric characterization is performed—such as sample dimensions, and modes used—are dictated by the requirements of the surface resistance measurement rather than optimizing the dielectric characterization itself. Despite this, the technique overcomes several limitations cited in earlier works [10]: accuracy in the determination of the parasitic losses in the metal walls of the cavity, and uncertainty in the unloaded quality factor measurement. The technique also includes a method for performing a weighted least-squares fit of the joint frequency and temperature dependence of the loss tangent and finding the uncertainty of the fitting parameters using a single dielectric sample. This overcomes the limitations of earlier techniques [20] which used several specimens of different sizes to achieve different resonant frequencies in a single-mode resonator and required uniformity in the dielectric samples used.

Our results for the relative permittivity of rutile crystals are comparable to previous works [9], [20]. An uncertainty of 0.7% has been achieved. The measured sample-to-sample differences cannot be attributed to the uncertainty

With respect to the loss tangent, for all crystals studied, we found a frequency and temperature dependence different from that stated in earlier publications [20] and different from that predicted by theory [21]. The results, however, support the empirical frequency dependence observed in nonorganic

ceramics in this frequency range [32]. We can fit our measured loss tangent data to obtain a joint frequency and temperature dependence with uncertainties below 13% from 6 to 10 GHz and 30 to 100 K. We find large sample-to-sample differences that cannot be attributed to measurement uncertainty and may become relevant when this material is included in resonators used for the characterization of RF loss of other materials, such as superconductors.

The described technique can be extended to characterize other high-permittivity dielectrics beyond rutile, with potential applications in Hakki–Coleman resonators used for quality control of metal and superconductive materials with limited sample sizes. This includes characterizing surface treatments for controlling secondary electron emission and other relevant effects at RF and microwave frequencies, applicable in particle accelerators, telecommunications, and other fields.

Appendix A
Calculation of Normalized Uncertainties

Suppose a multivariable function $z = F(x_1, x_2, x_3, \ldots, x_n)$ whose variables $x_1, x_2, x_3, \ldots, x_n$ are subject to experimental uncertainty. The uncertainty in z normalized to its nominal value satisfies the following equation:

$$\left(\frac{u_z}{z}\right)^2 = \left(\frac{\partial z}{\partial x_1}\frac{u_{x1}}{z}\right)^2 + \left(\frac{\partial z}{\partial x_2}\frac{u_{x2}}{z}\right)^2 + \cdots + \left(\frac{\partial z}{\partial x_n}\frac{u_{xn}}{z}\right)^2. \tag{13}$$

This general formula can be applied to relative permittivity and loss tangent.

A. Relative Permittivity

The sources of uncertainty in the relative permittivity (ϵ_r) primarily stem from the uncertainties in the diameter and height of the rutile crystal, as well as the repeatability of the frequency measurements. Accordingly, ϵ_r can be expressed as a function of these variables

$$\epsilon_r = F(D_r, L_r, f_0) \tag{14}$$

where D_r, L_r are the diameter and length of the rutile, and f_0 is the measured frequency. Thus, the square of the relative uncertainty is

$$\left(\frac{u_{\epsilon_r}}{\epsilon_r}\right)^2 = \left(\frac{\partial \epsilon_r}{\partial D_r}\frac{u_{D_r}}{\epsilon_r}\right)^2 + \left(\frac{\partial \epsilon_r}{\partial L_r}\frac{u_{L_r}}{\epsilon_r}\right)^2 + \left(\frac{\partial \epsilon_r}{\partial f_{\text{meas}}}\frac{u_{f\,\text{meas}}}{\epsilon_r}\right)^2 \tag{15}$$

which can be turned into (7) by defining the following sensitivity coefficients:

$$S_{D_r} = \frac{\partial \epsilon_r}{\partial D_r}\frac{D_r}{\epsilon_r}$$
$$S_{L_r} = \frac{\partial \epsilon_r}{\partial L_r}\frac{L_r}{\epsilon_r}$$
$$S_{f_0} = \frac{\partial \epsilon_r}{\partial f_0}\frac{f_0}{\epsilon_r}. \tag{16}$$

B. Loss Tangent

The sources of uncertainty in the loss tangent are mainly from the uncertainties dielectric filling factor, unloaded quality factor, surface resistance of Cu enclosure, and surface geometrical factor. Again, following (13), we have:

$$\left(\frac{u_{\tan\delta_r}}{\tan\delta_r}\right)^2 = \left(\frac{\partial \tan\delta_r}{\partial p_r}\frac{u_{p_r}}{\tan\delta_r}\right)^2 + \left(\frac{\partial \tan\delta_r}{\partial Q_0}\frac{u_{Q_0}}{\tan\delta_r}\right)^2 + \left(\frac{\partial \tan\delta_r}{\partial R_{s,\text{Cu}}}\frac{u_{R_s,\text{Cu}}}{\tan\delta_r}\right)^2 + \left(\frac{\partial \tan\delta_r}{\partial G_{s,\text{Cu}}}\frac{u_{G_s,\text{Cu}}}{\tan\delta_r}\right)^2. \tag{17}$$

From the equation above, (4) can be readily obtained by taking partial derivatives in (1) and (2).

Appendix B
Extension to Commercial Dielectrics

The purpose of this appendix is twofold: First, we aim to demonstrate that the procedure outlined in Section III is applicable to commercially available dielectrics commonly used in communication systems [34]. Second, we seek to show that dielectrics with significantly lower permittivity than rutile can also be effectively characterized using the cavities shown in Fig. 1. For this analysis, we assume a dielectric (DUT) with the same dimensions as the measured rutile samples ($D_r = 4.04$ mm, $L_r = 5.55$ mm), a relative permittivity of 20—typically the lowest value offered by manufacturers of dielectric materials for communications [34]—and a loss tangent of $1.67 \cdot 10^{-4}$ at 5.5 GHz [35]. Under these conditions, the PFs are 0.95 for the TE_{013} mode and 0.98 for the TE_{011} and TE_{012} modes. Consequently, the uncertainty in determining the loss tangent will primarily be dictated by the uncertainty in quality factor measurements.

Commercial dielectrics can have relative permittivities as high as 90 [34]. Permittivities greater than 20 will further increase the PFs, enabling the cavities shown in Fig. 1 to effectively characterize these materials across a wide range of temperatures and frequencies.

References

[1] B. W. Hakki and P. D. Coleman, "A dielectric resonator method of measuring inductive capacities in the millimeter range," *IEEE Trans. Microw. Theory Techn.*, vol. MTT-8, no. 4, pp. 402–410, Jul. 1960.

[2] C. Wilker, Z.-Y. Shen, V. X. Nguyen, and M. S. Brenner, "A sapphire resonator for microwave characterization of superconducting thin films," *IEEE Trans. Appl. Supercond.*, vol. 3, no. 1, pp. 1457–1460, Mar. 1993.

[3] J. Mazierska, "Dielectric resonator as a possible standard for characterization of high temperature superconducting films for microwave applications," *J. Supercond.*, vol. 10, no. 2, pp. 73–84, Apr. 1997.

[4] T. Puig et al., "Coated conductor technology for the beamscreen chamber of future high energy circular colliders," *Superconductor Sci. Technol.*, vol. 32, no. 9, Jul. 2019, Art. no. 094006, doi: 10.1088/1361-6668/ab2e66.

[5] A. Romanov et al., "High frequency response of thick REBCO coated conductors in the framework of the FCC study," *Sci. Rep.*, vol. 10, no. 1, p. 12325, Jul. 2020.

[6] A. Abada et al., "FCC-hh: The hadron collider: Future circular collider conceptual design report volume 3," *Eur. Phys. J. Special Topics*, vol. 228, no. 4, pp. 755–1107, 2019. [Online]. Available: https://link.springer.com/article/10.1140%2Fepjst%2Fe2019-900087-0

[7] P. Gan et al., "Design study of an YBCO-coated beam screen for the super proton-proton collider bending magnets," *Rev. Sci. Instrum.*, vol. 89, no. 4, Apr. 2018, Art. no. 045114.

[8] P. Krkotic, Q. Gallardo, N. D. Tagdulang, M. Pont, and J. M. O'Callaghan, "Algorithm for resonator parameter extraction from symmetrical and asymmetrical transmission responses," *IEEE Trans. Microw. Theory Techn.*, vol. 69, no. 8, pp. 3917–3926, Aug. 2021.

[9] J. Breeze, *Temperature and Frequency Dependence of Complex Permittivity in Metal Oxide Dielectrics: Theory, Modelling and Measurement*. Cham, Switzerland: Springer, 2016.

[10] J. Krupka, W.-T. Huang, and M.-J. Tung, "Complex permittivity measurements of low-loss microwave ceramics employing higher order quasi TE_{0np} modes excited in a cylindrical dielectric sample," *Meas. Sci. Technol.*, vol. 16, no. 4, pp. 1014–1020, Mar. 2005, doi: 10.1088/0957-0233/16/4/014.

[11] D. Kajfez and P. Guillon, *Dielectric Resonators*. Tucker, GA, USA: Noble Publishing Corporation, 1998.

[12] J. Krupka, D. Mouneyrac, J. G. Hartnett, and M. E. Tobar, "Use of whispering-gallery modes and quasi-TE_{0np} modes for broadband characterization of bulk gallium arsenide and gallium phosphide samples," *IEEE Trans. Microw. Theory Techn.*, vol. 56, no. 5, pp. 1201–1206, May 2008.

[13] (2018). *CST—Computer Simulation Technology, Dassault Systems*. [Online]. Available: https://www.cst.com/

[14] W. E. Courtney, "Analysis and evaluation of a method of measuring the complex permittivity and permeability microwave insulators," *IEEE Trans. Microw. Theory Techn.*, vol. MTT-18, no. 8, pp. 476–485, Aug. 1970.

[15] G. E. H. Reuter and E. H. Sondheimer, "The theory of the anomalous skin effect in metals," *Proc. Roy. Soc. London. Ser. A. Math. Phys. Sci.*, vol. 195, no. 1042, pp. 336–364, 1948.

[16] W. Chou and F. Ruggiero, "Anomalous skin effect and resistive wall heating. Lhc project note 2 (sl/ap)," CERN-Eur. Org. Nucl. Res., Meyrin, Switzerland, Tech. Rep., 1995. [Online]. Available: https://cds.cern.ch/record/691905/files/project-note-2.pdf and https://cds.cern.ch/record/691905

[17] J. Mazierska and C. Wilker, "Accuracy issues in surface resistance measurements of high temperature superconductors using dielectric resonators (corrected)," *IEEE Trans. Appiled Supercond.*, vol. 11, no. 4, pp. 4140–4147, Apr. 2001.

[18] N. M. Alford et al., "Dielectric loss of oxide single crystals and polycrystalline analogues from 10 to 320 k," *J. Eur. Ceram. Soc.*, vol. 21, no. 15, pp. 2605–2611, Jan. 2001.

[19] M. V. Jacob, J. Mazierska, K. Leong, and J. Krupka, "Microwave properties of low-loss polymers at cryogenic temperatures," *IEEE Trans. Microw. Theory Techn.*, vol. 50, no. 2, pp. 474–480, Feb. 2002, doi: 10.1109/22.982226.

[20] N. Klein et al., "Dielectric properties of rutile and its use in high temperature superconducting resonators," *J. Appl. Phys.*, vol. 78, no. 11, pp. 6683–6686, Dec. 1995.

[21] V. Gurevich and A. Tagantsev, "Intrinsic dielectric loss in crystals: Low temperatures," *Sov. Phys. JETP*, vol. 64, no. 142, pp. 142–151, 1986.

[22] G. W. Stewart, *Introduction To Matrix Computations*. Amsterdam, The Netherlands: Elsevier, Jun. 1973.

[23] (2023). *Alineason—Material & Technology*. [Online]. Available: https://www.alineason.com/

[24] P. Krkotic, A. Aguasca, and J. M. O'Callaghan, "Small footprint evaluation of metal coatings for additive manufacturing," in *Proc. 48th Eur. Microw. Conf. (EuMC)*, Sep. 2018, pp. 882–885.

[25] R. K. Kirby, "Thermal expansion of rutile from 100 to 700K," *J. Res. Natl. Bur. Stand. A Phys. Chem.*, vol. 71A, no. 5, pp. 363–369, 1967.

[26] T. H. K. Barron and G. K. White, *Heat Capacity and Thermal Expansion at Low Temperatures*. Boston, MA, USA: Springer, 1999, pp. 153–223.

[27] A. Okaya and L. Barash, "The dielectric microwave resonator," *Proc. IRE*, vol. 50, no. 10, pp. 2081–2092, Oct. 1962.

[28] M. E. Tobar, J. Krupka, E. N. Ivanov, and R. A. Woode, "Anisotropic complex permittivity measurements of mono-crystalline rutile between 10 and 300 k," *J. Appl. Phys.*, vol. 83, no. 3, pp. 1604–1609, Feb. 1998.

[29] N. Tagdulang, P. Krkotic, A. Diez, M. Pont, and J. M. O'Callaghan, "Accurate determination of dielectric properties in small, high-permittivity dielectric cylinders," in *Proc. 52nd Eur. Microw. Conf. (EuMC)*, Sep. 2022, pp. 95–98.

[30] E. S. Sabisky and H. J. Gerritsen, "Measurements of dielectric constant of rutile (TiO_2) at microwave frequencies between 4.2° and 300°K," *J. Appl. Phys.*, vol. 33, no. 4, pp. 1450–1453, Apr. 1962.

[31] A. Templeton, X. Wang, S. J. Penn, S. J. Webb, L. F. Cohen, and N. M. Alford, "Microwave dielectric loss of titanium oxide," *J. Amer. Ceram. Soc.*, vol. 83, no. 1, pp. 95–100, Jan. 2000.

[32] M. T. Sebastian, R. Ubic, and H. Jantunen, *Microwave Materials and Applications*. Hoboken, NJ, USA: Wiley, 2017.

[33] J. H. Lee, "'Measurements of the microwave loss of TiO_2 using an extremely high-Q sapphire-loaded cavity resonator with $YBa_2Cu_3O_{7-\delta}$ endplates," *J. Korean Phys. Soc.*, vol. 39, no. 6, pp. 1065–1071, 2001.

[34] *Dielectric Resonator Filters*. Hoboken, NJ, USA: Wiley, 2018, ch. 16, pp. 517–544, doi: 10.1002/9781119292371.ch16.

[35] (2024). *Trans-tech—Dielectrics*. [Online]. Available: https://www.trans-techinc.com/dielectrics//